**Article:**
Berrow, S.R., Mandle, R.J. and Gleeson, H.F. (Accepted: 2026) Synthesis and Properties of Liquid Crystalline Terphenyls containing a Difluorophenoxymethyl Moiety. Liquid Crystals. ISSN: 0267-8292 (In Press)

# Synthesis and Properties of Liquid Crystalline Terphenyls containing a Difluorophenoxymethyl Moiety

Stuart R. Berrow[a]*, Richard J. Mandle[a,b] and Helen F. Gleeson[a]

[a]*School of Physics and Astronomy, University of Leeds, Leeds, UK, LS2 9JT*

[b]*School of Chemistry, University of Leeds, Leeds, UK, LS2 9JT*

Stuart R. Berrow: https://orcid.org/0000-0003-3764-1613

Richard J. Mandle: https://orcid.org/0000-0001-9816-9661

Helen F. Gleeson: https://orcid.org/0000-0002-7494-2100

*Correspondence: S.R.Berrow@leeds.ac.uk

Word Count: 3973 (main text, excl. abstract, references etc.)

# Synthesis and Properties of Liquid Crystalline Terphenyls containing a Difluorophenoxymethyl Moiety

The synthesis of a series of liquid crystals based on a p-terphenyl core, substituted with an aliphatic ester at one terminus (with tail length varying from one to eleven repeat units) and a dilfuorophenoxymethyl moiety on the other, is reported. All materials in the series display an enantiotropic nematic phase, and for aliphatic tails of two or more repeat units also exhibit an enantiotropic smectic C phase. Both the nematic and smectic phase stability decrease with increasing tail length. There is also evidence for the presence of multiple soft crystal phases upon cooling in several of the materials. The optical properties of the materials are reported, with all materials showing maximum absorption wavelengths in the region of 334-337 nm, together with modest average refractive indices ($n_{av}$ = 1.55) and birefringence values of around 0.28.

Keywords: liquid crystals; terphenyls; Difluorophenoxymethyl; synthesis; optical properties.

## Introduction

Liquid crystalline materials have become a staple of everyday life, owing to their unique combination of properties which has made them excellent candidates for technologies such as displays[1,2]. For several of these technologies, the development of liquid crystal mixtures with desirable properties has been essential, to achieve performance not possible with single component materials[2]. Within these multi-component systems, p-terphenyls have found application, owing to properties such as the potential to have large dielectric anisotropy[3] and moderate-to-high optical birefringence[3,4] due to their large polarizability[5]. In particular, the incorporation of fluorinated p-terphenyls into liquid crystal mixtures has become commonplace[6–9]. Mixtures containing fluorinated p-terphenyls have been shown to have promise for application in optical devices[6] and terahertz technologies[7–9], to name a few. Thus, the development of novel fluorinated terphenyl structures attracts research

interest[3,10–12], and could provide opportunity to enhance the development of new liquid crystal mixtures.

The incorporation of the difluorooxymethylene bridge as a linking group in mesogenic compounds has been investigated over the last three decades[13], for example for the use in photonic devices with low response times[14]. In 2021, Manabe *et al* reported the synthesis and properties of a liquid crystal known as UUQU-4N, which contains a substituted difluorophenoxymethyl motif.[15] The reporting of UUQU-4N was significant as it was an early example of a material which displays the, then recently discovered, ferroelectric nematic ($N_F$) phase at low temperature (below 19.6 °C).[15] UUQU-4N is now considered to be one of the archetypal materials of the $N_F$ phase type[16], with its low phase transition temperatures (particularly melting point) attributed to the twisted conformation adopted by the difluorophenoxymethyl moiety.[17] As such, difluorophenoxymethyl motifs with varying substituents have become increasingly popular in liquid crystal chemistry in recent years[16–24], and have been implicated in the discovery of further liquid crystal phases[19,21,24]. Whilst an array of molecules have been explored both in academic[16–24] and patent literature[25–29], thus far, the incorporation of the difluorophenoxymethyl motif into p-terphenyl structures has been overlooked academically.

In this work, we report the synthesis of a series of liquid crystalline compounds based on a p-terphenyl core, which are substituted with the difluorophenoxymethyl moiety on one terminus, and an aliphatic ester tail on the other. Their liquid crystal phase behaviour is reported, and the effect of tail length on liquid crystal phase stability is discussed. We also examine the optical properties of the novel liquid crystalline terphenyls.

## Materials and Methods

### *Materials*

All chemical materials were used as purchased without further purification, and were obtained from either Apollo Scientific (Manchester UK), Fluorochem (Glossop, UK), or Merck (Gillingham, UK). Solvents were purchased from Merck (Gillingham, UK) and were used as received.

### *Material Synthesis*

Scheme 1 shows the synthetic pathway employed to yield the desired products $\mathbf{P_n}$ (where n represents the number of repeat units in the aliphatic tail). A generalised procedure for the synthesis of products $\mathbf{P_n}$ is given below. The synthetic procedure for the intermediates **I1** and **I2**, and spectral data for each product are given in the supplementary information.

*Generalised Esterification Procedure for Synthesis of Products ($P_n$)*

4-Hydroxy-(3’’,5’’-difluoro-4’’-(difluoro(3,4,5-trifluorophenoxy)methyl))-[1,1’:4’,1’’]-Terphenyl (0.48 g, 1 mmol), N,N'-dicyclohexylcarbodiimide 0.25 g, 1.2 mmol), 4-dimethylaminopyridine (12 mg, 0.1 mmol) and the appropriate carboxylic acid (1.2 mmol) were dissolved in tetrahydrofuran (10 mL) and stirred at room temperature overnight (>16h). The resulting mixture was diluted with chloroform (50 mL) and washed sequentially with water (50 mL), an aqueous solution of acetic acid (5%, 50 mL), brine (50 mL), before drying the organic phase over anhydrous magnesium sulphate. The crude material was then purified by flash column chromatography using a gradient of hexane to dichloromethane as eluent. The resulting solid was recrystallized from 2-propanol, to yield the product as colourless crystals.

### *Flash Chromatography*

Flash chromatography was performed on a Combiflash NextGen 300+ system (Teledyne Isco) using silica as a stationary phase (RediSep Silver; Teledyne Isco), an appropriate mobile phase as specified in the experimental procedure, and detection in the 200-800 nm wavelength range.

### *Structural Confirmation*

Nuclear magnetic resonance (NMR) spectra were recorded using a Bruker AVANCE III (400 MHz) NMR spectrometer (Bruker UK Ltd., Coventry, UK) at 298 K and referenced to TMS. NMR spectra were viewed and analysed using MNova NMR software.

Accurate Mass spectra were acquired on a Bruker Impact II QqTOF spectrometer using atmospheric pressure chemical ionisation (APCI). Samples were introduced using an HTC PAL autosampler and Bruker Elute Pump. HPLC columns were heated to 40 °C unless otherwise stated. Samples passed through a Bruker Diode array UV-detector before entering the mass spectrometer. Calibration was performed by infusion of 5 mM sodium formate solution at the end of each acquisition. Samples were submitted as solutions in acetonitrile at 10 µg/mL concentration, and data were collected in positive mode.

### *Thermal Analysis*

Differential scanning calorimetry (DSC) measurements were performed using a TA Instruments Q2000 DSC instrument (TA Instruments, Wilmslow UK), equipped with a RCS90 Refrigerated cooling system (TA Instruments, Wilmslow UK). The instrument was calibrated against an Indium standard, and data were processed using TA Instruments Universal Analysis Software. Samples were analysed under a nitrogen

atmosphere, in hermetically sealed aluminium TZero crucibles (TA Instruments, Wilmslow, UK) and subjected to three analysis cycles. For the analysis of the synthesised monomers (and intermediates) each cycle consisted of: a heating phase from 0–230 °C at a heating rate of 10 °C/min, an isothermal phase at 230 °C for 2 minutes, a cooling phase from 230-0 °C at 10 °C/min, and an isothermal phase at 0 °C for 2 minutes. All phase transitions are reported as peak values on the first heating cycle.

***Optical Microscopy***

Polarised light optical microscopy (POM) was performed using a Leica DM2700P polarised light microscope (Leica Microsystems (UK) Ltd., Milton Keynes, UK), equipped with 10x objective, and a rotatable stage. A Linkam LTS 350 heating stage (Linkam Scientific Instruments Ltd., Redhill, UK) equipped with a TMS 93 temperature controller (Linkam Scientific Instruments Ltd., Redhill, UK) was used for temperature variation. Images were recorded using a XIMEA UI-306x CP-C Camera (XIMEA GmbH, Münster, Germany) using IDS uEye Camera Software (IDS Imaging Development Systems Ltd, Farnham, UK). Samples were analysed sandwiched between untreated glass substrates, unless otherwise specified.

***X-ray Scattering Measurements***

2D Small angle (SAXS) and wide angle (WAXS) X-ray scattering experiments were performed on an Anton Paar SAXSpoint 5.0 system (K-α Cu source, λ=1.5418 Å) with a Dectris EIGER2 R 1M (1028 pixel x 1062 pixel array). Measurements were performed at the appropriate temperature, with the samples contained in QGCT 1.0 quartz capillaries (1.0 mm diameter; Capillary Tube Supplies Ltd., Cornwall, UK), averaging 3 frames with exposure times of 5 minutes each. A 2 mm beam size was

used. A background scan was performed for both the SAXS and WAXS detector position which was subtracted from the measurements to minimise contributions from intrinsic background scattering and the Mylar protective film in front of the detector. 2D data reduction was performed by radially integrating the 2D patterns whilst masking the central contribution related to the non-scattered X-ray beam. The instrument is calibrated against Silver Behenate, however due to the size of the capillary holder used, there is some flexibility in the position of the capillaries. which may give rise to some uncertainty in absolute q-values reported. This uncertainty may give rise to some uncertainty in absolute q-values reported, the extent of which depends on the sample-to-detector distance at which the experiments are conducted; however, in this work we focus on relative positions, not strictly absolute values, thus do not believe any potential errors influence our results or conclusions.

***Absorption Spectra***

Absorption spectra were recorded using an Edinburgh Instruments FL1000 Fluorimeter (Edinburgh, UK) in Transmission mode. Samples were dissolved in acetonitrile at a concentration of 5 μM, and contained within quartz cuvettes. Spectra were acquired with a 0.1 s dwell time at each wavelength (1 nm increments), over the range of 200-800 nm, with the final spectra being averaged over three acquisitions.

***Liquid Crystal Cells***

Liquid crystal alignment cells were obtained from Instec Inc (Boulder, CO, USA). For visualisation of liquid crystal textures and birefringence measurements, the cells used were treated to produce planar alignment and had nominal cell gaps of 2 μm and 4 μm respectively. For current reversal measurements, the cells used contain no alignment layer and have a nominal cell thickness of 10 μm.

## Results and Discussion

### *Phase Transition Analysis*

The phase transition temperatures observed for the products are displayed graphically in Figure 1**,** and detailed in Table S1. In general, the materials reported herein have relatively high melting points, as high as 182.5 °C for **P1**, owing to the terphenyl nature of the materials. Increasing tail length (n) leads to reductions in melting point, with a melting point plateau in the region of 85-95 °C for $n \geq 8$. The materials all exhibit a reasonable degree of supercooling, with as much as a 30.2 K difference in melting and crystallisation temperatures (**P4**) at a heating/cooling rate of 10 °C/min.

#### *Nematic Phase*

Regardless of the length of the tail, all samples exhibit an enantiotropic nematic phase, with **P2** exhibiting the widest nematic phase range, from 158.6 °C to 218.6 °C. In the case of **P1**, the nematic phase is the only mesophase observed, attributed to the acetyl terminal chain giving little scope for lipophilic interactions and thereby supressing layer formation. In general, as the length of the tail is increased, nematic phase stability decreases, with a plateau being approached for $n \geq 8$ where the effect of tail length on molecular anisotropy is diminished. There is also evidence of weak-odd even effects for $2 \leq n \leq 8$, which are attributed to the odd numbered terminal tails effectively extending molecular anisotropy, compared to even numbered tails effectively reducing the anisotropy.

The assignment of the nematic phase throughout the series was determined based on POM and X-ray observations. When examined between untreated substrates, upon cooling from the isotropic phase into the nematic phase, a schlieren texture is observed immediately at the phase transition (Figure 2b)). This texture quickly

transitions into largely optically isotropic appearance (Figure 2c)), with localised regions of schlieren texture showing low birefringence colours. These observations suggest that in the nematic phase, the materials of these series preferentially align homeotropically when untreated substrates are employed in sample preparation. When examined in cells treated to yield antiparallel planar alignment (Figure 2d)), all samples display uniform alignment throughout, as is typical for aligned nematic materials. When examined via wide-angle x-ray scattering (WAXS), all samples exhibit scattering patterns characteristic of the nematic phase, with diffuse lobes at high q indicating a preferential orientation (Figure 2a and Figure S1-S11), and no significant small angle features, as confirmed by radial integration (Figure S13).

*Smectic C Phase*

For $n \geq 2$, all members of the series present an enantiotropic smectic C phase. Upon cooling from the homeotropic nematic phase, the emergence of a schlieren texture showing birefringence colours is observed (Figure 3b)). The emergence of higher order birefringence colours suggests a transition from a near homeotropically aligned state to tilted alignment, consistent with a smectic C phase. When examined in cells treated to yield antiparallel planar alignment, the smectic C phase shows a characteristic domain texture (Figure 3c), of domains of alternating tilt angles. Further to the POM images, WAXS scattering patterns display sharp Bragg reflections in the small angle region (Figure S14) and diffuse lobes at higher q values, which are not orthogonal to each other (Figure 3a)). This suggests a tilt of the director relative to the layer normal and is characteristic of the smectic C phase.

The potential of a tilted structure is further evidenced by a change in the q position of small angle scattering features, which shift to higher values upon entering the smectic C phase. Using the weak SAXS features observed in the nematic phase as a

measure of the end-to-end molecular length, which will be of the order of the average molecular length, the shift to higher q values in the smectic phase represents a reduction in the length scale (Figure S15). A tilt of the director would therefore be needed to accommodate such a change in spacing, and in the case of the samples analysed in Figure S15, this tilt is in the region of 23-30°. This angle is in agreement with estimates from qualitative examination of the X-ray scattering figures.

To further probe this tilt angle, molecular lengths were computed for a range of low energy conformers of molecules P1-P11 generated using the GOAT algorithm[30] in ORCA 6.1[31] using the r2scan-3c composite DFT method[32]. Boltzmann weighting using the SCF energy of each conformer gives the average molecular length, which are reported in Table S2. Comparing these molecular lengths to the real-space position of the small angle Bragg peak supports the assignment of a tilted structure, as the average molecular lengths are larger than the observed layer spacings in all cases. The tilt angles based on the calculated molecular lengths are in the region of 43-50°, larger than that reported based on the small angle nematic scattering feature. It is of note that the average end-to-end molecular lengths are computed in the gas phase using a single molecule in isolation. As the alkyl tail length increases, there is a greater probability of a single *gauche* conformation being adopted, which in turn can be stabilised due to favourable tail-tail interactions through back-bending. This leads to the non-monotonic increase in molecular lengths observed in Table S2, and will influence the tilt angle calculated.

Whilst there are differences in the tilt angle depending on the method used, the presence of a tilted orientation of mesogens in these compounds is clear, supporting the assignment of a smectic C phase. It is of note that tilt angles reported in the smectic C phase are often in the region of 10-30°[33], and are dependent on several factors. In

particular, the nature of the tilt in smectic C systems is strongly influenced by the phase transition sequence prior to the transition to the smectic C phase[33,34]. Compounds that exhibit a direct isotropic or nematic to smectic C transition are often found to have larger tilt angles[34], which show minimal temperature related variation[33]. In contrast, if the transition into the smectic C phase is second order, for example from a smectic A phase, there is significant temperature dependence[33,35]. Given that P2-P11 all show direct nematic to smectic C transitions, the lack of temperature dependence on tilt angle/layer spacings observed in this work (Figure S15) are in agreement with previous literature findings.

As n is increased, the smectic C phase stability generally decreases, albeit to a much lesser extent than is observed for the nematic phase and melting point, with $T_{SmC-N}$ falling from 158.6 °C for **P2**, to 135.6 °C for **P11**. It is generally expected that longer terminal tails promote lipophilic interactions and thereby promote smectic layer formation. Thus, the decrease in smectic phase stability observed is surprising. We hypothesise that the observed decrease in smectic C phase stability may be the result of increased steric hinderance imparted by the increasingly long tails. Such hindrance may limit the ability of neighbouring molecules to approach sufficiently closely to promote layer formation. Thus, lower temperatures, at which the chains have slightly less conformational freedom, are required to allow the formation of layers, hence a reduction in $T_{SmC-N}$.

As is observed for the nematic phase, there is also some weak evidence of odd-even effects for $3 \leq n \leq 8$ in smectic C phase stability. Given the prevalence of polar liquid crystal phases in compounds containing the difluorooxymethylene bridge, we felt it prudent to confirm the apolar nature of the smectic C (and nematic) phase in these

materials through current reversal measurements. In all cases, no evidence of polar order was observed, with an example of the current response shown in Figure S16.

*Further Observations*

On cooling, several of the materials in this series exhibit multiple exothermic transitions during DSC analysis (Figure S1-S11 panel a)), often in relatively quick succession, notably in **$P_2$**, **$P_3$** and **$P_7$-$P_{11}$**. In all but one case, these transitions are all significant exothermic events, suggesting multiple crystallisation events, and thus the presence of soft crystal phases. POM evidence also supports the presence of multiple crystal phases (Figure S12), with transitions between mosaic textures and more conventional crystal appearance observed. Based on the textures, these appear to be some combination of soft crystal G/H phases, however without the ability to undertake X-ray studies on well aligned samples, identification of the nature of these soft crystal phases is not feasible.

In the case of P10, at 68.0 °C, a small exothermic event is observed in the DSC (Figure S10a)), suggesting the presence of another liquid crystal phase. However, POM investigations show the development of a mosaic texture, reminiscent of the soft crystal textures observed for other samples. These observations suggest that this other possible liquid crystal phase is a product of supercooling that could not be reproduced under microscopy conditions. Given that this phase forms from a smectic C phase, it is likely that the phase would be either a smectic I or smectic F.

***Optical Properties***

Terphenyl structures have often found use in liquid crystal mixtures for device applications, both due to their ability to form liquid crystal phases, as well as their interesting optical and photo-physical properties[1,3,6,9]. As a representative group for this novel series of materials, the birefringence (Δn) of **$P_2$**, **$P_5$**, **$P_7$** and **$P_9$** was examined

on cooling using a Berek compensator, with the results displayed in Figure 4.

In all cases, subsequent to the transition from the isotropic phase to the nematic phase, the birefringence is seen to increase sharply, followed by a steady increase in the nematic phase as temperature decreases. Upon the transition to the smectic C phase, the birefringence generally undergoes a step change, at which point a plateau is seen in Δn. The step change observed upon the transition from N to SmC is attributed to the increase in orientational order and packing density associated with the formation of lamellar structures within the material.[17] This step change is indicative of a first order phase transition, in agreement with the nature of the SmC to N transition observed via DSC. It is of note that the step change in birefringence is less pronounced upon entering the smectic C phase in $P_2$ than in the other materials. This is attributed to the nematic-to-smectic C transition in $P_2$ being more second-order like (i.e. having lower enthalpy and occurring over a broader temperature range) than for the other materials examined (see Table S1 and Figure S2a). This thus explains the more continuous behaviour of the optical properties, like birefringence than in the other materials.

For each of the materials examined in Figure 4, the maximum recorded birefringence plateaus in the region of 0.26-0.29 in the smectic C phase. Whilst there are small differences between samples, the birefringence of these materials is consistent irrespective of tail length, as expected given the optical properties of liquid crystalline materials are dominated by the mesogenic core, which remains unchanged. It has previously been reported that the presence of the $-CF_2-O-$ group lowers birefringence, as it disrupts conjugation and thus polarizability along the length of the molecule, as well as adopting a distorted conformation that reduces packing density.[17] Thus, the modest Δn values observed for the materials in this series are in agreement with observations reported in previous literature.

With the birefringence of the materials characterised, attempts to quantify the refractive indices of **P2** were undertaken, utilising a guest-host method and extrapolating the values of the ordinary and extraordinary refractive indices ($n_o$ and $n_e$ respectively). Mixtures of varying quantities of **P2** in E7 were made, and their refractive indices measured as a function of temperature using an Abbé refractometer. The refractive index values used for extrapolation were recorded at the same reduced temperature relative to the nematic to isotropic transition ($T_C$) of the sample. This reduced temperature is 0.913 x $T_C$, based on recording the refractive index values of E7 at 30 °C (303.15 K) and the $T_C$ of E7 being 59 °C (332.15 K). The extrapolated plot is given in Figure S21.

The extrapolated values for $P_2$ suggest that at 176 °C (the appropriate reduced temperature relative to the clearing temperature of $P_2$ at which the E7 mixtures were analysed), $P_2$ has an $n_e$ of 1.67 and an $n_o$ of 1.48, corresponding to an average refractive index ($n_{av}$) of 1.55 and a birefringence of 0.19. This is comparable to the Δn value obtained from Berek compensator measurements, in which the Δn observed at 176 °C is 0.23. These results therefore suggest that as well as modest birefringence values, $P_2$ and likely the entire series, has modest refractive indices.

In addition to the measurement of birefringence and refractive indices, absorption spectra were run for each of the products (Figure S22-S32). As is typical of terphenyl structures, in all cases, the materials show a strong absorbance in the UV region, with $\lambda_{max}$ vales in the region of 334-337 nm. Furthermore, all samples show no noticeable absorbance in the visible region of the spectrum, consistent with their colourless appearance.

## Conclusions

This work has reported the synthesis of a novel series of substituted [1,1':4',1'']-

Terphenyls, containing a difluorophenoxymethyl substituent, and varying in the length of their terminal tail. In all cases, the materials display enantiotropic liquid crystallinity, with nematic and smectic C phases for all materials containing two or more repeat units in their terminal tail, and only a nematic phase when the terminal tail consists of a single methyl group. Surprisingly, not only does increasing terminal tail length decrease melting point and nematic phase stability, but also leads to a decrease in smectic C phase stability, contrary to typical observations.

Regardless of terminal tail length, the birefringence of the materials appears to plateau in the region of 0.28 in the smectic C phase. Abbe refractometry measurements using a guest host method support the birefringence values recorded, and suggest the materials have modest refractive indices, with an average refractive index in the nematic phase of 1.55. We hypothesise that, whilst no polar phases are observed in this series, the addition of further fluorine substituents in the terphenyl unit could provide the necessary electron density profile to promote polar ordering.

**Supporting Materials**

The following are available as supporting materials: Synthetic procedure for synthesis of 3,5-difluoro-4-(difluoro(3,4,5-trifluorophenoxy)methyl)phenylboronoic acid pinacol ester; synthetic procedure for the synthesis of 4-Hydroxy-*(3'',5''-difluoro*-4''-*(difluoro(3,4,5-trifluorophenoxy)methyl))*-[1,1':4',1'']-Terphenyl; structural characterisation of all products ($P_n$); phase confirmation for all final products; polarised light optical microscopy confirmation of the presence of multiple crystal phases; layer spacings as a function of temperature; average molecular end-to-end lengths for all products; representative current reversal measurements; refractive index measurements for $P_2$; absorption spectra for all products.

## Author Contributions

Conceptualization, S.R.B; methodology, S.R.B and H.F.G.; validation, S.R.B; formal analysis, S.R.B; investigation, S.R.B.; resources, S.R.B. and R.J.M; data curation, S.R.B; writing—original draft preparation, S.R.B.; writing—review and editing, S.R.B, R.J.M, H.F.G.; visualization, S.R.B; supervision, H.F.G.; project administration, S.R.B and H.F.G.; funding acquisition, H.F.G. and R.J.M. All authors have read and agreed to the published version of the manuscript.

## Acknowledgements

The authors would like to acknowledge Prof. Mark Wilson for useful discussions. S.R.B and H.F.G acknowledge funding from the Engineering and Physical Sciences Research Council, grant number EP/V054724/1. R.J.M acknowledges UKRI FLF grant number MR/W006391. The authors also acknowledge the Engineering and Physical Sciences Research Council grant number EP/X0348011 for the purchase of the SAXS/WAXS system used in this work. The funders had no role in the design of the study; in the collection, analyses, or interpretation of data; in the writing of the manuscript; or in the decision to publish the results.

## Data Availability Statement

The data underlying this study are openly available in 'Dataset associated with Synthesis and Properties of Liquid Crystalline Terphenyls containing a Difluorophenoxymethyl Moiety', available at https://doi.org/10.5518/1839.

## Disclosure Statement

There are no conflicts to declare.

## References


[1] Kirsch P, Bremer M. Nematic liquid crystals for active matrix displays: Molecular design and synthesis. Angew Chem Int Ed. 2000;39(23):4216–4235.

[2] Lee SH, Bhattacharyya SS, Jin HS, et al. Devices and materials for high-performance mobile liquid crystal displays. J Mater Chem. 2012;22(24):11893–11903.

[3] Wan D, Che Z, Mo L, et al. Synthesis and properties of fluorinated terphenyl liquid crystals utilizing 5,6-dihydro-4H-cyclopenta[b]thiophene as core unit. J Mol Struct. 2022;1267:133612.

[4] Chen Y, Sun J, Xianyu H, et al. High birefringence fluoro-terphenyls for thin-cell-gap TFT-LCDs. J Disp Technol. 2011;7(9):478–481.

[5] Zang ZQ, Zhang D, Wan XH, et al. Synthesis and property of liquid crystalline 4-alkoxyl-4″-cyano-p-terphenyls. Mol Cryst Liq Cryst Sci Technol, Sect A. 2000;339:145–158.

[6] Hird M. Fluorinated liquid crystals – properties and applications. Chem Soc Rev. 2007;36(12):2070–2095.

[7] Wang L, Lin X, Liang X, et al. Large birefringence liquid crystal material in terahertz range. Opt Mater Express. 2012;2(10):1314.

[8] Reuter M, Garbat K, Vieweg N, et al. Terahertz and optical properties of nematic mixtures composed of liquid crystal isothiocyanates, fluorides and cyanides. J Mater Chem C Mater. 2013;1(29):4457–4463.

[9] Trushkevych O, Xu H, Lu T, et al. Broad spectrum measurement of the birefringence of an isothiocyanate based liquid crystal. Appl Opt. 2010;49(28):5212–8216.

[10] Song K, Li J, Li J, et al. New terphenyl liquid crystals terminated by 2-chloro-3,3,3-trifluoropropenyl group. Liq Cryst. 2017;44(11):1646–1652.

[11] Valdés-Pech MA, Larios-López L, Rodríguez-González RJ, et al. Semi-fluorinated p-terphenyl liquid crystals. J Fluor Chem. 2019;218:42–50.

[12] Wang K, Rai P, Fernando A, et al. Synthesis and properties of fluorine tail-terminated cyanobiphenyls and terphenyls for chemoresponsive liquid crystals. Liq Cryst. 2020;47(1):3–16.

[13] Kirsch P, Bremer M, Taugerbeck A, et al. Difluorooxymethylene-Bridged Liquid Crystals: A Novel Synthesis Based on the Oxidative Alkoxydifluorodesulfuration of Dithianylium Salts. Angewandte Chemie. 2001;113(8):1528–1532.

[14] Peng Z, Liu Y, Cao Z, et al. Fast response property of low-viscosity difluorooxymethylene-bridged liquid crystals. Liq Cryst. 2013;40(1):91–96.

[15] Manabe A, Bremer M, Kraska M. Ferroelectric nematic phase at and below room temperature. Liq Cryst. 2021;48(8):1079–1086.

[16] Cruickshank E. The Emergence of a Polar Nematic Phase: A Chemist's Insight into the Ferroelectric Nematic Phase. Chempluschem. 2024;89(5):e202300726.

[17] Song Y, Huang X, Zhang X, et al. Ferroelectric Nematic Liquid Crystals Showing High Birefringence. Advanced Science. 2025;12(9):2414317.

[18] Berrow SR, Hobbs J, Gibb CJ. Reactive Fluid Ferroelectrics: A Gateway to the Next Generation of Ferroelectric Liquid Crystalline Polymer Networks. Small. 2025;21(21):2501724.

[19] Gibb CJ, Hobbs J, Nikolova DI, et al. Spontaneous symmetry breaking in polar fluids. Nat Commun. 2024;15(1):5845.

[20] Strachan GJ, Górecka E, Hobbs J, et al. Fluorination: Simple Change but Complex Impact on Ferroelectric Nematic and Smectic Liquid Crystal Phases. J Am Chem Soc. 2025;147(7):6058–6066.

[21] Pociecha D, Szydlowska J, Vaupotič N, et al. Twist Grain Boundary Phases in Proper Ferroelectric Liquid Crystals Realm. Advanced Science. 2025;12(38):e08405.

[22] Strachan GJ, Górecka E, Pociecha D. Competition between mirror symmetry breaking and translation symmetry breaking in ferroelectric liquid crystals with increasing lateral substitution. Mater Horiz. 2026;13:779–785.

[23] Strachan GJ, Ramsay SJ, Juodka M, et al. Interplay of Polar Order and Positional Order in Liquid Crystals–Observation of Re-entrant Ferroelectric Nematic Phase. Angew Chem Int Ed. 2025;64(46):e202516302.

[24] Strachan GJ, Górecka E, Szydłowska J, et al. Nematic and Smectic Phases with Proper Ferroelectric Order. Advanced Science. 2025;12(3):2409754.

[25] Tanaka H. Pentacyclic liquid crystal compound having CF2O bonding group, liquid crystal composition and liquid crystal display. European Patent Office; 2008.

[26] 张伟, 孟劲松, 员国良, et al. Liquid crystal compounds containing dimethylbenzene and difluoromethyleneoxy linking groups and their applications. China; 2015.

[27] 智広 矢野, 智広 矢野, 山下　淳一, et al. Liquid crystal compound, liquid crystal composition and liquid crystal display element having CF2OCF3 at terminal. Japan; 2013.

[28] Tanaka H, Endou H. Composé à cristaux liquides ayant un groupe difluorométhylèneoxy, composition à cristaux liquides et élément d'affichage à cristaux liquides. European Patent Office; 2014.

[29] 道子 高橋, さや香 藤森, 笹田 康幸. Liquid crystal compound having cf2o bonding group and tolane backbone, liquid crystal composition, and liquid crystal display element. WIPO (PCT); 2015.

[30] de Souza B. GOAT: A Global Optimization Algorithm for Molecules and Atomic Clusters. Angew Chem Int Ed. 2025;64(18).

[31] Neese F. The ORCA program system. Wiley Interdiscip Rev Comput Mol Sci. 2012;2(1):73–78.

[32] Grimme S, Hansen A, Ehlert S, et al. r2SCAN-3c: A "Swiss army knife" composite electronic-structure method. J Chem Phys. 2021;154(6).

[33] Trittel T, Harth K, Stannarius R. Smectic C to smectic A transition induced mechanically by the rupture of freely suspended liquid crystal films. Soft Matter. 2017;13(17):3199–3204.

[34] Koden M, Anabuki T, Nakagawa K, et al. Tilt Angle Behavior of Smectic C Phase in Binary Systems. Jpn J Appl Phys. 1991;30(6B):1129–1131.

[35] Kapernaum N, Hartley CS, Roberts JC, et al. Systematic variation of length ratio and the formation of smectic A and smectic C phases. ChemPhysChem. 2010;11(10):2099–2107.

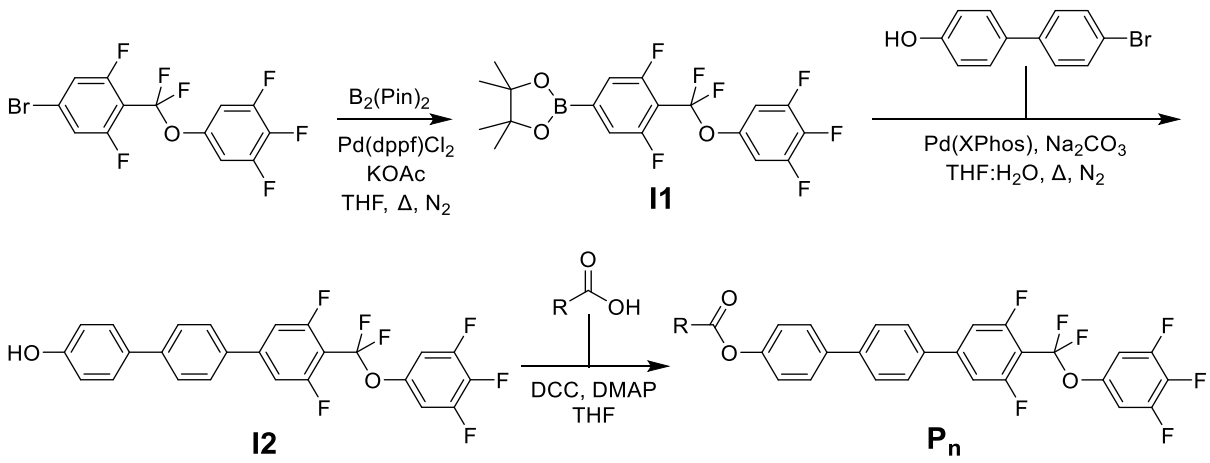


Scheme 1 – The synthetic route employed in the synthesis of the final compounds in this work. (The final products are denoted $P_n$ where n denotes the number of methylene units on the alkyl tail, represented in as R in the scheme).

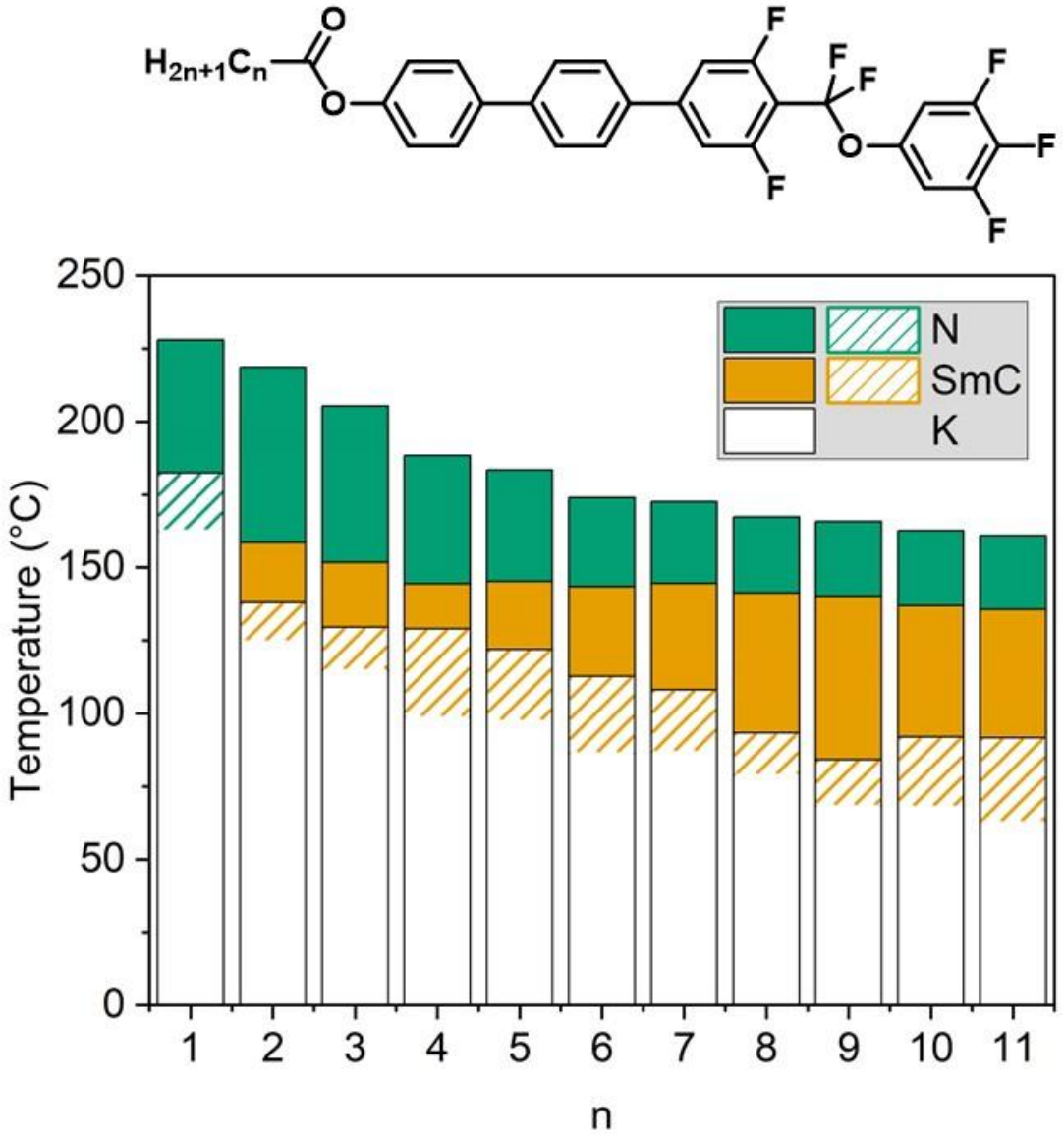


Figure 1 – The phase transition temperatures of the product series as a function of alkyl chain length (n), illustrated in the chemical structure atop the figure. The graph depicts the temperature ranges over which each phase is observed, recorded via DSC at a heating/cooling rate of 10 °C/min, with hashed areas denoting temperatures over which the phase is observed due to supercooling.

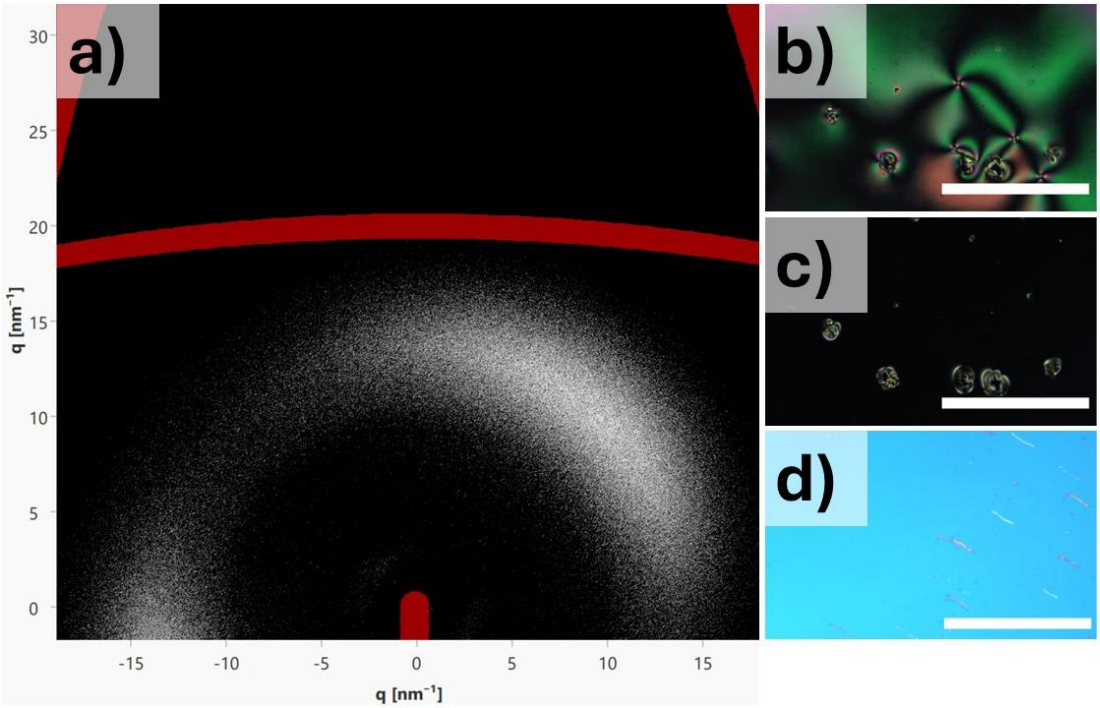


Figure 2 – a) an example of the 2D WAXS scattering pattern obtained in the nematic phase of $P_1$, showing anisotropic lobes in the wide angle region; b) the schlieren texture observed for $P_1$ between untreated glass substrates immediately upon transitioning into the nematic phase at 227 °C from the isotropic phase and c) the optically isotropic appearance observed for the same sample in the nematic phase with homeotropic alignment after cooling away from the transition temperature at 225 °C (in both cases the scale bar denotes 250 µm); d) a sample of $P_2$ in the nematic phase at 190 °C in a cell treated to yield antiparallel planar alignment (scale bar denotes 500 µm).

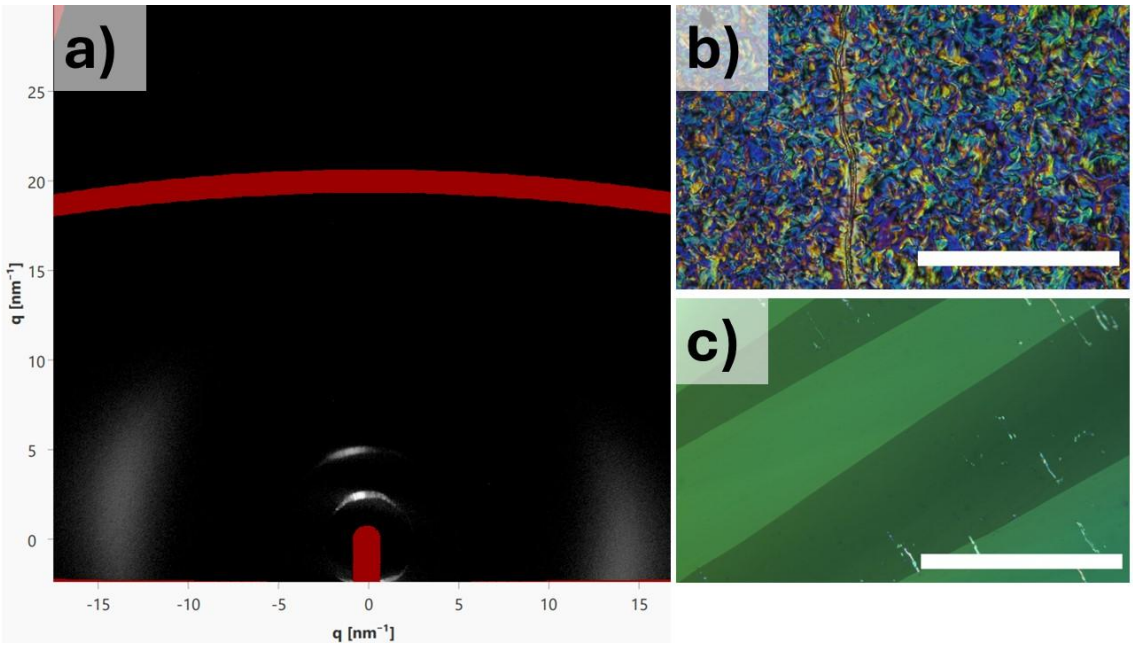


Figure 3 – a) an example of the 2D WAXS scattering pattern obtained in the smectic C phase, in this case recorded for $P_6$ at 125 °C, showing sharp Bragg reflections in the small angle region and anisotropic lobes in the wide angle region; the SAXS and WAXS features are not orthogonal, suggesting a tilted smectic structure; b) An example of the schlieren texture typical of a smectic C phase, observed for $P_6$ at 133 °C when viewed between untreated glass slides (scale bar denoted 250 μm); c) An example of the domain texture observed in the smectic C phase of $P_2$ at 150 °C when in a cell treated for antiparallel planar alignment (scale bar denotes 500 μm).

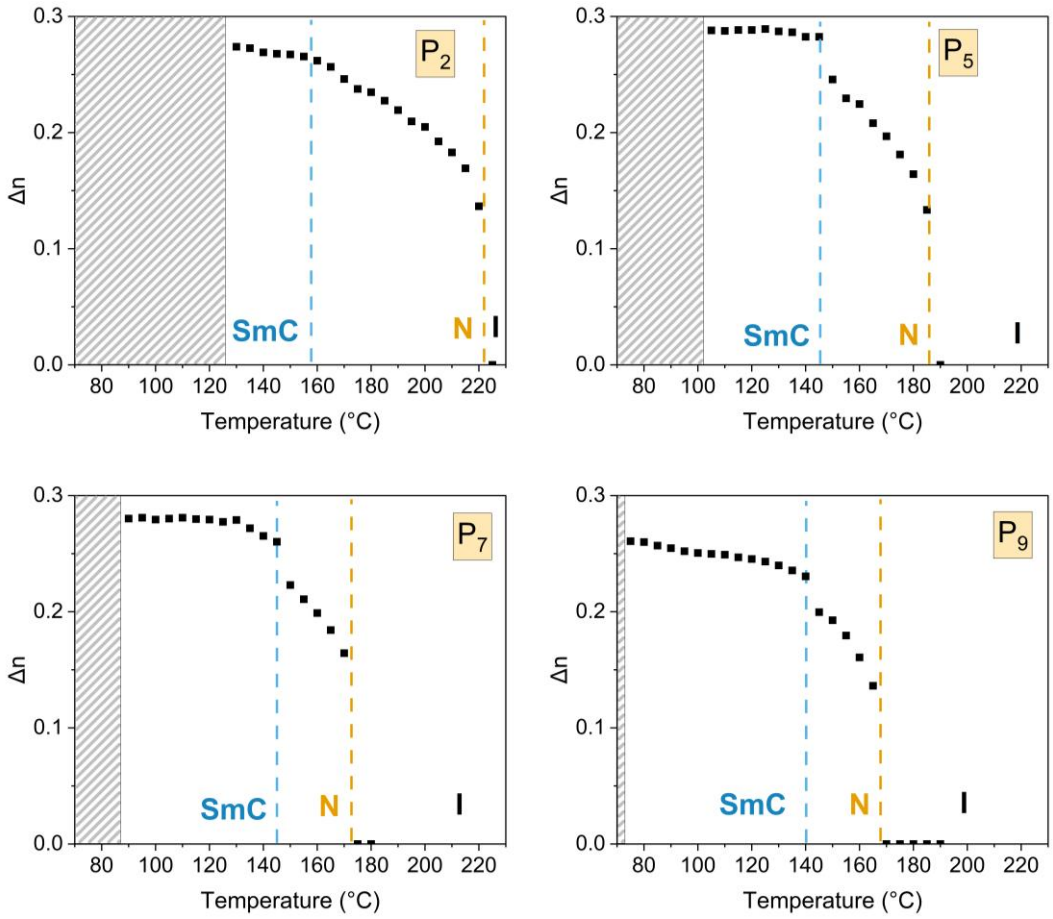


Figure 4 – The birefringence (Δn) as a function of temperature observed for $P_2$, $P_5$, $P_7$ and $P_9$ upon cooling from the isotropic phase. The transition from isotropic to the nematic phase is marked by the orange dashed line, and the transition from the nematic to smectic C phase is marked by the blue dashed line. The area marked by the grey shaded box denotes crystallisation of the sample.